



Negative-Pressure Enhanced Ferroelectricity and Piezoelectricity in Lead-free BaTiO₃ Ferroelectric Nanocomposite Films

Journal:	<i>Journal of Materials Chemistry C</i>
Manuscript ID	TC-ART-03-2020-001556.R2
Article Type:	Paper
Date Submitted by the Author:	12-May-2020
Complete List of Authors:	Zhang, Xiyuan; Nanjing University of Aeronautics and Astronautics Xu, Ruixing; Nanjing University of Aeronautics and Astronautics Gao, Xingyao; Purdue University Ji, Yanda; Nanjing University of Aeronautics and Astronautics, Department of Applied Physics Qian, Fengjiao; Nanjing University of Aeronautics and Astronautics Fan, Jiyu; Magnetism group, applied physics Wang, Haiyan; Purdue University System, MSE; Neil Armstrong Engineering Building Li, Weiwei; University of Cambridge, Department of Materials Science & Metallurgy Yang, Hao; Nanjing University of Aeronautics and Astronautics, College of Science

Negative-Pressure Enhanced Ferroelectricity and Piezoelectricity in *Lead-free* BaTiO₃ Ferroelectric Nanocomposite Films

Xiyuan Zhang,^a Ruixing Xu,^a Xingyao Gao,^b Yanda Ji,^a Fengjiao Qian,^a Jiyu Fan,^{*,a} Haiyan Wang,^b Weiwei Li^{*,c} and Hao Yang^{*,a,d}

^aCollege of Science, Nanjing University of Aeronautics and Astronautics, Nanjing 211106, P. R. China. E-mail: jiyufan@nuaa.edu.cn, yanghao@nuaa.edu.cn

^bSchool of Materials Engineering, Purdue University, West Lafayette, IN 47907, USA

^cDepartment of Materials Science & Metallurgy, University of Cambridge, 27 Charles Babbage Road, Cambridge, CB3 0FS, United Kingdom. E-mail: w1337@cam.ac.uk

^dKey Laboratory for Intelligent Nano Materials and Devices of the Ministry of Education, Nanjing University of Aeronautics and Astronautics, Nanjing 211106, P. R. China

Due to environmental concerns and the increasing drive towards miniaturization of electronic circuits and devices, *lead-free* ferroelectric films with low leakage current and robust ferroelectric and piezoelectric are highly desired. The preferred alternative, BaTiO₃, is non-toxic and has ferroelectric property, but its high leakage current, poor ferroelectric and piezoelectric and low Curie temperature of ~ 130 °C in *thin film* form are obstacles for the high-temperature practical applications. Here, we report that negative-pressure-driven enhancement of ferroelectric Curie temperature and effective piezoelectric coefficient are achieved in (111)-oriented BaTiO₃ nanocomposite films. The enhanced ferroelectric and piezoelectric properties in emergent monoclinic BaTiO₃ are attributed to the sharp vertical interface and 3D tensile strain that develops by interspersing stiff and self-assembled vertical Sm₂O₃ nanopillars through film thickness. Our work also demonstrates that fabricating oxide films through (111)-oriented epitaxy open the door to the creation of new phase components and exploration of novel functionalities for developing oxide quantum electronic devices.

1. Introduction

Ferroelectrics possess a polarization that is spontaneous, stable and electrically switchable.¹ Due to strongly coupling between their electrical, mechanical, thermal, and optical responses, ferroelectrics have been widely investigated for a diverse range of applications such as non-volatile memory devices, sensors, capacitors, non-linear optical components, piezoelectric actuators, energy harvesting and storage, micro-electromechanical systems, and high-power electronic transducers.²⁻⁶ Over the past decades, industry-standard ferroelectric materials are based on $\text{Pb}_{1-x}\text{Zr}_x\text{TiO}_3$ and contain *lead*, which is toxic and environmentally unfriendly.⁷ In consideration of the growing demand for green materials with minimized impacts on health and environment, *lead-free* alternative materials are urgently needed.^{8,9} Further, with the increasing drive towards miniaturization of electronic circuits and devices, stable piezoelectric and ferroelectric with high Curie temperature and low leakage current in film form are highly required. The preferred alternative, BaTiO_3 , is non-toxic and has ferroelectric property, but its high leakage current, poor piezoelectric and ferroelectric and low Curie temperature of ~ 130 °C in *thin film* form limit the high-temperature practical applications of electronic devices.^{10,11} Biaxial strain has been used to enhance the Curie temperature of epitaxial BaTiO_3 films, but only for thicknesses of tens of nanometers,¹² which are not thick enough for some device applications. Also, high leakage current and large coercive field reported in plain BaTiO_3 films pose significant challenges for achieving low-voltage operation and low power consumption in electronic devices.¹³⁻¹⁷

Benefiting from the advances in substrate preparation techniques,¹⁸ an interesting proposition is to rely on higher index surfaces such as (111).¹⁹ Since its structure resembles a buckled honeycomb lattice similar to two-dimensional (2D) materials, the symmetry and interactions across epitaxial (111) interfaces have led to novel phenomena such as a polar metal phase in NdNiO₃ films,²⁰ exchange bias in LaNiO₃-LaMnO₃ superlattices,²¹ and two-dimensional topological insulators.²² Note that different crystallographic orientations can give rise to diverging interfacial coupling and resulting properties. For ferroelectric thin films, theoretical studies of in-plane strain applied along the (111) plane have predicted that the spontaneous polarization and Curie temperature of BaTiO₃ are insensitive to compressive strain, but can be significantly enhanced by tensile strain (> 2.5%).²³⁻²⁵ However, there are very few experimental results because the very limited commercial (111)-oriented substrates can be used for imposing such large tensile strain. Furthermore, similar to well-studied (001)-oriented ferroelectric films, the in-plane (111) strain can only be maintained for thicknesses of tens of nanometers, which are not robust enough for many applications.

Recently, density-functional theory calculations predicted the enhanced ferroelectric properties for PbTiO₃ and BaTiO₃ ferroelectrics under negative pressure (or hydrostatic tensile stress).²⁶ By using the difference in the density of PbTiO₃ in the different phases, Wang *et al.* reported the negative-pressure-driven enhancement of ferroelectric and piezoelectric properties in free-standing PbTiO₃ and Pb(Zr,Ti)O₃ nanowires.^{27,28}

Nevertheless, the effects of negative pressure associated with ferroelectric films grown

along the (111) direction with hexagonal symmetry have received less attention. This is because horizontal strain engineering of ferroelectric thin films in layered heterostructures is incapable of expansion in three mutually perpendicular directions, that is, negative pressure. A novel method to achieve negative pressure control in much thicker films involves the growth of self-assemble vertical nanocomposites.²⁹⁻³² In YBa₂Cu₃O_{7- δ} :BaZrO₃ nanocomposite films, in-plane and out-of-plane lattice expansion (or negative pressure) have been demonstrated in YBa₂Cu₃O_{7- δ} phase, with a strong modification of superconductive properties.^{31,33}

Here, we report the nanocomposite films of BaTiO₃:Sm₂O₃ grown on (111)-oriented 0.5 wt.% Nb-doped SrTiO₃ substrates that generate negative pressure in the BaTiO₃. It was found that rare earth element may diffuse in ferroelectrics.^{34,35} Sm₂O₃ was selected as the second phase for the strain controlling because it have been confirmed that it substitutes very minimally into the BaTiO₃.¹⁴ Besides, Sm₂O₃ has a large elastic modulus of 125 GPa, compared to 67 GPa for BaTiO₃ and is very insulating.^{32,36,37} In 500-nm-thick films, we demonstrate negative-pressure-driven enhancement of the ferroelectric Curie temperature, from 130 °C to 616 °C, large longitudinal effective piezoelectric coefficient d_{33}^{eff} (~ 80 pm V⁻¹) in the emergent monoclinic BaTiO₃. Such enhancements of ferroelectric and piezoelectric properties in thick films open a new door to using BaTiO₃ in high-temperature ferroelectric film applications.

2. Experimental details

Pulsed laser deposition was used to grow high-quality plain BaTiO₃ and

(BaTiO₃)_{0.5}:(Sm₂O₃)_{0.5} nanocomposite films on (111)-oriented 0.5 wt.% Nb-doped SrTiO₃ substrates. The growth temperatures were optimized at 800 °C, with the oxygen partial pressure of 0.25 mbar, with a laser fluence of 1-2 J cm⁻², and at a laser repetition rate of 2-4 Hz. The distance between target and substrate was set to 8 cm. All films were cooled at a rate of 5 °C min⁻¹ to ambient temperature in a static-oxygen pressure of 0.8 atm. High-resolution four circle X-ray diffraction (Panalytical Empyrean, K α radiation) and scanning transmission electron microscopy (STEM, FEI Tecnai F20 analytical microscope) were used to investigate the crystallographic of thin films.

Top Au electrodes with an area of 3.14×10^{-4} cm² were sputtered for the dielectric measurements. Dielectric permittivity was calculated from the measured capacitance (C) using $C = \epsilon_0 \epsilon_r A / d$, where A is the area of the top electrode and d is the thickness of the film. The dielectric measurements were using Impedance Analyzer (E4990A). For the ferroelectric measurements, top Au electrodes with an area of 7.85×10^{-5} cm² were deposited by the sputtering. Ferroelectric hysteresis loops were measured by a Radiant Precision materials analyzer. The temperature was controlled by a Linkam Scientific Instruments HFS600E-PB4 system. Piezoresponse force microscopy measurements were conducted using Asylum Research AFM MFP-3D origin with an Environmental Controller and a HVA220 High Voltage Amplifier. The Environment Controller, HVA220 High Voltage Amplifier and the ARC2 Controller were connected in series, and the sample was placed on the variable temperature holder. The temperature can be raised to the target temperature and the maximum temperature for the stability test was 200 °C.

3. Results and discussion

Figure 1a shows X-ray diffraction (XRD) θ - 2θ scans of plain BaTiO₃ film and BaTiO₃:Sm₂O₃ nanocomposite film, revealing that all films are epitaxial and without intermixed crystalline phases. Compared to plain BaTiO₃ film, the BaTiO₃ peak in nanocomposite films shifts towards low angle indicating an increase of out-of-plane lattice parameter. To minimize the out-of-plane lattice mismatch and interfacial energy with (111) Nb:STO, BaTiO₃ and Sm₂O₃ exhibit (111) and (224) orientations in the nanocomposite films, respectively. This result is confirmed by selected area diffraction (SAD) image which also reveals in-plane orientations for (110)_{BTO}||((110)_{STO}||((004)_{Sm2O3}) and (001)_{BTO}||((001)_{STO}||((220)_{Sm2O3}) (Figure S1). From scanning transmission electron microscopy (STEM) images (Figure 1b and S1), we can see that self-assembled Sm₂O₃ nanopillars are distributed and embedded in a BaTiO₃ matrix. Also, an interface without visible misfit dislocation is formed along the interface between BaTiO₃ and Sm₂O₃ (Figure S1). To examine the change of lattice parameters for (111)-oriented films, X-ray reciprocal space maps (RSMs) studies were applied and results are shown in Figure 1c. From a combination of θ - 2θ scans and RSMs, the lattice parameters of a, b, and c were calculated and are presented in Table 1. In plain BaTiO₃ film, the in-plane lattice parameters are same to BaTiO₃ bulk and out-of-plane lattice parameter is slightly larger than that of BaTiO₃ bulk.³⁸ This indicates that stoichiometric BaTiO₃ films were fabricated. It was reported that the increase of out-of-plane lattice parameter can be induced by an increase of out-of-plane domains when the BaTiO₃ film domain pattern gets more distorted.³⁹ The tilted lattices and nanodomains can be further formed by the

ferroelectric distortion. As a consequence, the lattice parameters can be increased through the phase transition.⁴⁰ In BaTiO₃:Sm₂O₃ nanocomposite film, due to the stiff Sm₂O₃ nanopillars with diameters of 3~5 nm are embedded in a BaTiO₃ matrix, we found that the lattice constants of a, b, and c in BaTiO₃ are increased (Table 1), indicating that negative pressure is formed in nanocomposite films. The lattice angles of α , β , and γ are further calculated by $\cos\theta = \frac{\vec{a}\cdot\vec{b}}{|\vec{a}||\vec{b}|}$, yielding $\alpha = \gamma = 90^\circ$ and $\beta = 99.01^\circ$ for BaTiO₃ in nanocomposite films (Table 1). Together with the observation of lattice parameters $a \neq b \neq c$, it has been revealed that BaTiO₃ has a monoclinic structure (Figure S2), in consistent with tensile strain-driven a monoclinic structure predicted by the density-functional theory calculation.²³⁻²⁶

To explore negative pressure effect on Curie temperature of BaTiO₃, temperature-dependent XRD studies are presented in Figure 2a and Figure S4. Temperature-dependent evolution of lattice parameter d_{222} reveals two regimes over the temperature range from 25-900 °C separated by a kink that is characteristic of a phase transition. The presence of phase transitions at ~180 °C, ~368 °C, and ~616 °C for plain BaTiO₃ film, 100 nm and 500 nm nanocomposite films, respectively, are observed. For the plain BaTiO₃ film, the transition is close to BaTiO₃ bulk (~130 °C).¹¹ Whereas, for a 500-nm-thick nanocomposite film, the phase transition is significantly enhanced to be ~616 °C. To verify that phase transitions observed in the XRD studies, we probed the temperature dependence of the dielectric permittivity (Figure 2b). For plain BaTiO₃ film, a broad peak is observed and Curie temperature is determined to be ~160 °C. The value is

similar to plain (001)-oriented BaTiO₃ film reported in the literatures.^{14,41,42} For a 500-nm-thick nanocomposite film, we observed that the Curie temperature is ~563 °C. These values are in agreement with the phase transition measured from XRD studies and confirm the presence of a ferroelectric-to-paraelectric phase transition at these temperatures. We conclude that, owing to negative pressure, the Curie temperature of BaTiO₃ is strongly enhanced from ~130 °C to ~616 °C in the 500-nm-thick nanocomposite film.

From ferroelectric hysteresis measurements, a 500-nm-thick nanocomposite film was confirmed to be ferroelectric to at least 300 °C (Figure 3a). A robust remanent polarization (P_r) of 23 $\mu\text{C cm}^{-1}$, which was calculated using the area of the BTO component in the nanocomposite film, was recorded both at room temperature and 300 °C. The room temperature value is significantly higher than that of plain BaTiO₃ film (Figure S5), and similar to (001)-oriented BaTiO₃ films from literatures.^{14,16,17,43} The high piezoelectricity found in PbZr_{1-x}Ti_xO₃ and related PbTiO₃ solid solutions materials originates in the existence of a monoclinic crystal structure and the formation of nanodomains at the morphotropic phase boundary (MPB).⁴⁴⁻⁴⁶ Thus, ferroelastic nanodomain structures and low-symmetry monoclinic phases are helpful for inducing large piezoelectricity. In ferroelectric films, epitaxial strain also offers the possibility to enhance the effective piezoelectric properties (d_{33}^{eff}) utilizing low crystal symmetries and high density of domain walls.³⁹ Note that reducing the domain size can improve the effective piezoelectric properties (d_{33}^{eff}) in the (111)-oriented BaTiO₃ single

crystals.⁴⁷ Piezoresponse force microscopy (PFM) was further applied to explore the piezoelectricity in the 500-nm-thick nanocomposite film. Although it is a daunting challenge to accurately measure the effective piezoelectric coefficient (d_{33}^{eff}) through PFM, several works have reported the measurement of effective values for d_{33}^{eff} .⁴⁸⁻⁵⁰ While, some other proofs have been sought to demonstrate the inherent difficulties associated with quantitative d_{33}^{eff} .⁵¹⁻⁵⁵ As discussed in these literatures, the selection of the cantilever, the uncertainty of the contact between the tip coating and tip surface and electrostatic effects all lead to the decrease of the credibility of PFM as a quantitative tool. Considering these factors, some preventive measures were firstly taken to minimize the negative impact. Measurements were carried out on the same position of the same sample with same cantilever and same laser spot position on the cantilever backside which are known to affect the results. Electrostatic effects were considered to be ignored due to the relatively stiff cantilever used (1.4-5.8 N/m) and the grounding of samples. To obtain the deformation of the piezoelectric material due to the application of the voltage, the switching spectroscopy PFM (SS-PFM) was conducted to give the measured piezoresponse amplitude as a function of driving frequency, f ,

$$A(f) = \frac{f_0^2 A_d}{\sqrt{(f_0^2 - f^2)^2 + \left(\frac{f_0 f}{Q}\right)^2}} \quad (1)$$

where A_d is the amplitude of the electric-field-induced deformation driving the system, Q is the quality factor and f_0 is the resonant frequency. In addition, SS-PFM measurements was performed in the dual AC resonance tracking (DART) mode, which used two excitation frequencies f_1, f_2 and led to four measured quantities, namely the corresponding amplitudes A_1, A_2 and phases Φ_1, Φ_2 . As a result, the A_d can be

calculated from the obtained values of Q and f_0 .⁵⁶ Effective piezoelectric coefficient d_{33}^{eff} was extracted from $A_d = d_{33}^{eff} V_{ac}$, where V_{ac} is a drive amplitude. Besides, it is worth noting that, in the conventional approach, PFM amplitude and phase are acquired at a fixed frequency, which are insufficient for the determination of a full characteristic of the tip-surface junction in the framework of a simple harmonic oscillator (SHO) model.^{53,54} A SHO model is characterized by resonance frequency, which amplitude and phase at the resonance frequency and Q -factor are independent. But, in single-frequency PFM, only two independent parameters, i.e., the amplitude and phase, are measured at a fixed frequency, and therefore are inadequate to describe the system completely. In this work, multiple frequencies are selected to determine the SHO model parameters for the tip-surface junction. The response is measured over the same band of frequency, and Fourier transformed to get amplitude, and phase as function of frequency. However, this approach will inevitably enhance the piezoelectric response by increasing the signal noise ratio due to resonance. As shown in Figure S6, SHO fitting was used to reduce the increase of signal noise ratio caused by the resonance and quantify the accurate A_d .

With the limitation of the instrument (PFM sample heater) and stability of the PFM cantilevers used, robust butterfly loops of piezoelectricity and phase hysteresis loops were obtained with PFM spectroscopic measurements from room temperature to 200 °C (Figure 3b). As discussed above, although it is still very difficult to quantify d_{33} by PFM, a non-decreasing effective piezoelectric coefficient (d_{33}^{eff}) with a value of ~ 80

pm V⁻¹ is measured from room temperature to 200 °C, indicating strong and stable piezoelectricity in BaTiO₃:Sm₂O₃ nanocomposite films. Meanwhile, the value (~ 80 pm V⁻¹) is the highest effective piezoelectric coefficient ever recorded compared with that of BaTiO₃ films measured using PFM.⁵⁷⁻⁵⁹ Also, compared to (111)-oriented plain BaTiO₃ films,^{60,61} our (111)-oriented BaTiO₃:Sm₂O₃ nanocomposite films have the largest effective piezoelectric coefficient and relative high ferroelectric Curie temperature.

Based on the aforementioned discussion and results, a crystallographic model of the vertical interface between BaTiO₃ and Sm₂O₃ is presented in Figure 4a. Due to negative pressure (or 3D tensile strain) applied along the three dimension (Figure 4b), in this case, the three oxygen atoms around Ti atom move away from each other and open an empty space at the center of the oxygen triangle, which allows Ti atom to move off-center and then can significantly enhance ferroelectric Curie temperature. This is consistent with (111) BaTiO₃:Sm₂O₃ nanocomposite films, compared to plain (111) BaTiO₃ films. Figure 4c shows the theory calculation of the in-plane strain phase diagram for (111)-oriented BaTiO₃.²⁴ We can see that the ferroelectric Curie temperature is enhanced by the tensile strain and the monoclinic phase is also stabilized under the tensile strain.^{24,62} In addition, the enhanced ferroelectric Curie temperature of (111)-oriented BaTiO₃ in nanocomposite films is equivalent to that of plain (111)-oriented BaTiO₃ films applied by an in-plane strain value of ~ 4.5%, which is impossible achieved in the plain films.

4. Conclusions

In summary, strongly enhanced ferroelectricity and piezoelectricity were achieved in self-assembled nanocomposite films of BaTiO₃ and Sm₂O₃. The strong and robust remanent polarization and effective piezoelectric coefficient can be maintained to at least 300 °C and 200 °C, respectively. The enhancement of ferroelectric Curie temperature (~616 °C) and effective piezoelectric coefficient (~80 pm V⁻¹) is attributed to negative pressure generated by the strain coupling between stiff Sm₂O₃ nanopillars and surrounding BaTiO₃ matrix. Through (111)-oriented epitaxial films, our results demonstrate a new promising route to creating negative pressure and developing *lead-free* ferroelectric films with the formation of new phase components, which improve their Curie temperature and exploitable properties for applications. The enhanced ferroelectric and piezoelectric properties in BaTiO₃ may also enable the development of energy efficient quantum electronic devices.

Author contribution

H.Y and W.-W.L supervise the project. X.Z fabricated the samples and carried out XRD, AFM, piezoelectric and ferroelectric measurements with the support from R.X, Y.J, F.Q and J.F. X.G and H.W performed the STEM measurements. X.Z, W.-W.L and H.Y prepared the manuscript with the contribution from all authors.

Conflicts of interest

There are no conflicts to declare.

Acknowledgements

This work was supported by the National Nature Science Foundation of China (Grant No.U1632122, 11774172, and 51602152), Postgraduate Research & Practice Innovation Program of Jiangsu Province (KYCX18_0243), and the Open Fund of Key Laboratory for Intelligent Nano Materials and Devices of the Ministry of Education INMD-2019M06. X.G. and H.W. acknowledge the support from the U. S. National Science Foundation for the TEM work (DMR-1565822).

References

- 1 M. Dawber, K. M. Rabe and J. F. Scott, *Rev. Mod. Phys.* 2005, **77**, 1083.
- 2 G. H. Haertling, *J. Am. Ceram. Soc.* 1999, **82**, 797-818.
- 3 N. Setter, D. Damjanovic, L. Eng, G. Fox, S. Gevorgian, S. Hong, A. Kingon, H. Kohlstedt, N. Y. Park, G. B. Stephenson, I. Stolitchnov, A. K. TagansteV, D. V. Taylor, T. Yamada and S. Streiffer, *J. Appl. Phys.* 2006, **100**, 051606.
- 4 G. Catalan and J. F. Scott, *Adv. Mater.* 2009, **21**, 2463.
- 5 J. F. Scott, *Science* 2007, **315**, 954-959.
- 6 Y.-M. You, W.-Q. Liao, D. Zhao, H.-Y. Ye, Y. Zhang, Q. Zhou, X. Niu, J. Wang, P.-F. Li, D.-W. Fu, Z. Wang, S. Gao, K. Yang, J.-M. Liu, J. Li, Y. Yan and R.-G. Xiong, *Science* 2017, **357**, 306-309.
- 7 M. D. Maeder, D. Damjanovic and N. Setter, *J. Electroceramics* 2004, **13**, 385-392.
- 8 E. Cross, *Nature* 2004, **432**, 24.
- 9 D. Damjanovic, N. Klein, J. Li and V. Porokhinskyy, *Funct. Mater. Lett.* 2010, **3**, 5.
- 10 T. Takenaka and H. Nagata, *J. Eur. Ceram. Soc.* 2005, **25**, 2693.
- 11 M. Zgonik, P. Bernasconi, M. Duelli, R. Schlessner, P. Günter, M. H. Garrett and D. Rytz, *Phy. Rev. B* 1994, **50**, 5941.
- 12 K. J. Choi, M. Biegalski, Y. L. Li, A. Sharan, J. Schubert, R. Uecker, P. Reiche, Y. B. Chen, X. Q. Pan, V. Gopalan, L.-Q. Chen, D. G. Schlom and C. B. Eom, *Science* 2004, **430**, 758.
- 13 H. Zheng, J. Wang, S. E. Lofland, Z. Ma, L. Mohaddes-Ardabili, T. Zhao, L. Salamanca-Riba, S. R. Shinde, S. B. Ogale, F. Bai, D. Viehland, Y. Jia, D. G. Schlom, M. Wuttig, A. Roytburd and R. Ramesh, *Science* 2004, **303**, 661.
- 14 S. A. Harrington, J. Zhai, S. Denev, V. Gopalan, H. Wang, Z. Bi, S. A. T. Redfern, S.-H. Baek, C. W. Bark, C.-B. Eom, Q. Jia, M. E. Vickers and J. L. MacManus-Driscoll, *Nat. Nanotechnol.* 2011, **6**, 491.
- 15 A. Kursumovic, E. Defay, O. J. Lee, C.-F. Tsai, Z. Bi, H. Wang and J. L. MacManus-Driscoll, *Adv. Funct. Mater.* 2013, **23**, 5881.
- 16 F. Khatkhatay, A. Chen, J. H. Lee, W. Zhang, H. Abdel-Raziq, and H. Wang, *ACS Appl. Mater. Interfaces* 2013, **5**, 12541.
- 17 A. Dasgupta, S. Saremi, R. Xu, L. Dedon, S. Pandya, A. P. Damodaran and L. W. Martin, *J. Mater. Chem. C* 2018, **6**, 10751.
- 18 J. Chang, Y.-S. Park and S.-K. Kim, *Appl. Phys. Lett.* 2008, **92**, 152910.
- 19 J. Chakhalian, A. J. Milli and J. Rondinelli, *Nat. Mater.* 2012, **11**, 92.
- 20 T. H. Kim, D. Puggioni, Y. Yuan, L. Xie, H. Zhou, N. Campbell, P. J. Ryan, Y. Choi, J. W. Kim, J. R. Patzner, S. Ryu, J. P. Podkaminer, J. Irwin, Y. Ma, C. J. Fennie, M. S. Rzchowski, X. Q. Pan, V. Gopalan, J. Rondinelli and C.-B. Eom, *Nature* 2016, **533**, 68.
- 21 M. Gibert, P. Zubko, R. Scherwitzl, J. Íñiguez and J.-M. Triscone, *Nat. Mater.* 2012, **11**, 195.
- 22 D. Xiao, W. Zhu, Y. Ran, N. Nagaosa, and S. Okamoto, *Nat. Commun.* 2011, **2**,

- 596.
- 23 R. Oja, K. Johnston, J. Frantti and R. M. Nieminen, *Phys. Rev. B* 2008, **78**, 094102.
 - 24 H. Wu, X. Ma, Z. Zhang, J. Zeng, J. Wang and G. Chai, *AIP Adv.* 2016, **6**, 015309.
 - 25 T. Angsten, L. W. Martin and M. Asta, *Phys. Rev. B* 2017, **95**, 174110.
 - 26 S. Tinte, K. M. Rabe and D. Vanderbilt, *Phys. Rev. B* 2003, **68**, 144105.
 - 27 J. Wang, B. W. Eerd, T. Sluka, C. Sandu, M. Cantoni, X.-K. Wei, A. Kvasov, L. McGilly, P. Gemeiner, B. Dkhil, A. Tagantsev, J. Trodahl and N. Setter, *Nat. Mater.* 2015, **14**, 985.
 - 28 A. Kvasov, L. McGilly, J. Wang, Z. Shi, C. Sandu, T. Sluka, A. Tagantsev and N. Setter, *Nat. Commun.* 2016, **7**, 12136.
 - 29 V. Moshnyaga, B. Damaschke, O. Shapoval, A. Belenchuk, J. Faupel, O. Lebedev, J. Verbeeck, G. Tendeloo, M. Mücksch, V. Tsurkan, R. Tidecks and K. Samwer, *Nat. Mater.* 2003, **2**, 247.
 - 30 J. L. MacManus-Driscoll, P. Zerrer, H. Wang, H. Yang, J. Yoon, A. Fouchet, R. Yu, M. Blamire and Q. Jia, *Nat. Mater.* 2008, **7**, 314.
 - 31 R. Zhao, W.-W. Li, J. Lee, E.-M. Choi, Y. Liang, W. Zhang, R. Tang, H. Wang, Q. Jia, J. L. MacManus-Driscoll and H. Yang, *Adv. Funct. Mater.* 2014, **24**, 5240.
 - 32 W.-W. Li, R. Zhao, R. Tang, A. Chen, W. Zhang, X. Lu, H. Wang and H. Yang, *ACS Appl. Mater. Interfaces* 2014, **6**, 5356.
 - 33 W.-W. Li, L. Wang, R. Zhao, R. Tang, Y. Liang and H. Yang, *J. Appl. Phys.* 2014, **116**, 183904.
 - 34 P. Du, L. Luo, W.-P. Li and Q.-Y. Yue *J. Appl. Phys.* 2014, **116**, 014102.
 - 35 F. Li, M. J. Cabral, B. Xu, Z.-X. Cheng, E. C. Dickey, J. M. LeBeau, J.-L. Wang, J. Luo, S. Taylor, W. Hackenberger, L. Bellaiche, Z. Xu, L.-Q. Chen, T. R. Shrout and S.-J. Zhang. *Science*. 2019, **364**, 264.
 - 36 R. G. Munro, *Elastic Moduli Data for Polycrystalline Ceramics* 6853 (NISTIR, 2002).
 - 37 IEEE. *Proceedings of the 5th International Symposium on Micro Machine and Human Science* 75 (Nagoya, 1994).
 - 38 G. H. Kwei, A. C. Lawson, S. J. L. Billinge and S.-W. Cheong, *J. Phys. Chem.* 1993, **97**, 2368.
 - 39 A. S. Everhardt, S. Matzen, N. Domingo, G. Ctalan and B. Noheda, *Adv. Electron. Mater.* 2016, **2**, 1500214.
 - 40 T. Shimizu, D. Suwama, H. Taniguchi, T. Taniyama and M. Itoh, *J. Phys.: Condens. Matter* 2013, **25**, 132001.
 - 41 Y. Shintani and O. Tada, *J. Appl. Phys.* 1970, **41**, 2376.
 - 42 K. Iijima, T. Terashima, K. Yamamoto, K. Hirata and Y. Bando, *Appl. Phys. Lett.* 1990, **56**, 527.
 - 43 K. Abe, S. Konatsu, N. Yanase, K. Sano and T. Kawakubo, *Jpn. J. Appl. Phys.* 1997, **36**, 5846.
 - 44 B. Noheda, J. A. Gonzalo, L. E. Cross, R. Guo, S.-E. Park, D. E. Cox and G. Shirane, *Phys. Rev. B* 2000, **61**, 8687.
 - 45 L. Bellaiche, A. Garcia and D. Vanderbilt, *Phys. Rev. Lett.* 2000, **84**, 5427.
 - 46 Y. M. Jin, Y. Wang, A. G. Khachatryan, J. F. Li and D. Viehland, *Phys. Rev. Lett.*

- 2003, **91**, 197601.
- 47 K. Yao, H. Kakemoto, T. Tsurumi and S. Wada, *Mater. Sc. Eng. B* 2005, **120**, 181.
- 48 Z. H. Zhou, X. S. Gao, J. Wang, K. Fujihara, S. Ramakrishna and V. Nagarajan, *Appl. Phys. Lett.* 2007, **90**, 052902.
- 49 V. Nagarajan, A. Roytburd, A. Stanishevsky, S. Prasertchoung, T. Zhao, L. Chen, J. Melngailis, O. Auciello and R. Ramesh, *Nat. Mater.* 2003, **2**, 43-47.
- 50 A. G. Agronin, Y. Rosenwaks and Gil I. Rosenman, *Nano Lett.* 2003, **3**, 169-171.
- 51 A. Labuda, and R. Proksch, *Appl. Phys. Lett.* 2015, 106, 253103.
- 52 T. Jungk, Á. Hoffmann and E. Soergel, *Appl. Phys. Lett.* 2007, 91, 253511.
- 53 B. Y. Huang, E. N. Esfahani and J. Y. Li, *Nat. Sci. Rev.* 2019, **6**, 55-63
- 54 Q. F. Zhu, E. N. Esfahani, S. H. Xie and J. Y. Li, *Theo & Appl Mech Lett.* 2020, **10**, 23-26.
- 55 T. Jungk, Á. Hoffmann and E. Soergel, *Appl. Phys. Lett.* 2006, 89, 163507.
- 56 A. Gannepalli, D. G. Yablon, A. H. Tsou and R. Proksch, *Nanotech.* 2013, **24**, 355705.
- 57 I.-D. Kim, Y. Avrahami, H. L. Tuller, Y.-B. Park, M. J. Dicken and H. A. Atwater, *Appl. Phys. Lett.* 2005, **86**, 192907.
- 58 B. C. Luo, D. Y. Wang, M. M. Duan and S. Li, *Appl. Phys. Lett.* 2013, **103**, 122903.
- 59 A. Piorra, A. Petraru, H. Kohlstedt, M. Wuttig and E. Quandt, *J. Appl. Phys.* 2011, **109**, 104101.
- 60 Z. Wang, L. Yan, Y. Yang, J. Li, J. Das, A. L. Geiler, A. Yang, Y. Chen, V. G. Harris, and D. Viehland, *J. Appl. Phys.* 2011, **109**, 034102.
- 61 C. Deng, Y. Zhang, J. Ma, Y. Lin, and C.-W. Nan, *Acta Mater.* 2008, **56**, 405.
- 62 A. Raeliarijaona and H. Fu, *J. Appl. Phys.* 2014, **115**, 054105.

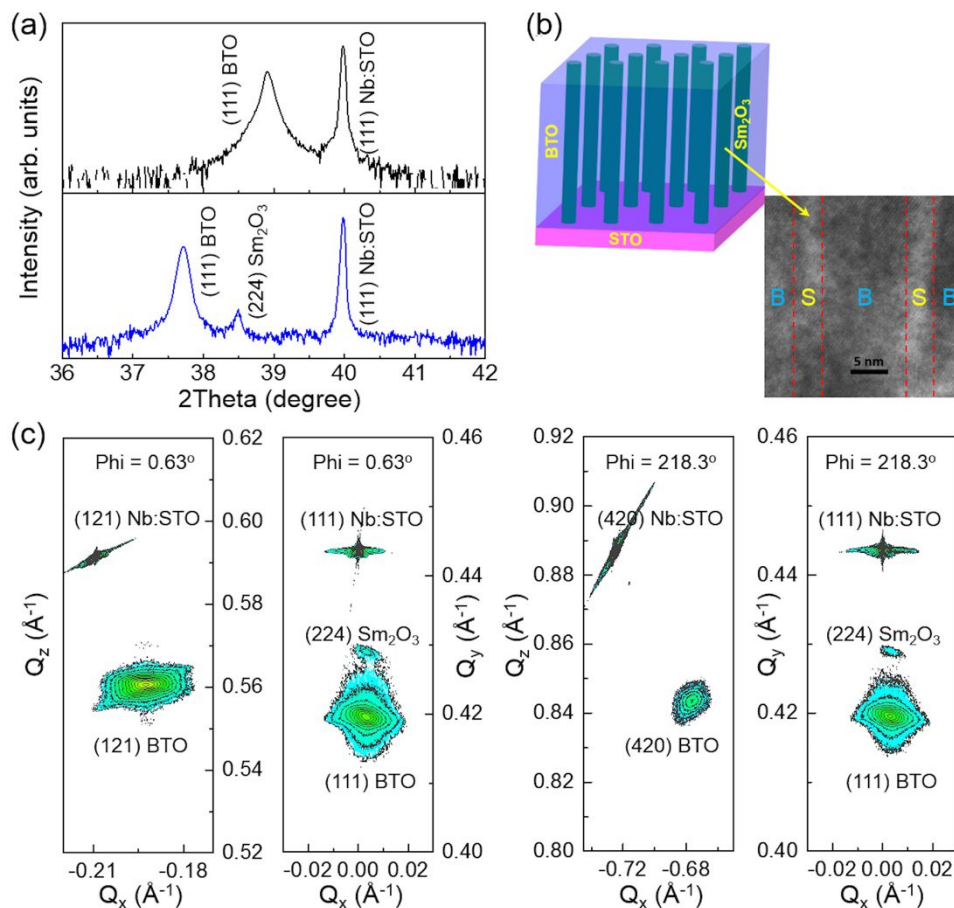


Figure 1. (a) XRD θ - 2θ scans for plain BaTiO₃ 100 nm film and BaTiO₃:Sm₂O₃ 500 nm nanocomposite film grown on (111) Nb:SrTiO₃. (b) Top panel: a schematic diagram of VAN structure. Bottom panel: cross-sectional STEM image of BTO:Sm₂O₃ film. B is BTO and S is Sm₂O₃. (c) X-ray reciprocal space maps (RSMs) of (121), (420), and (111) Bragg reflections of Nb:SrTiO₃, BaTiO₃, and Sm₂O₃ at $\Phi = 0.63^\circ$ and $\Phi = 218.3^\circ$ for calculating the lattice parameters and lattice angles of BaTiO₃ in 500-nm-thick nanocomposite film. Φ is an azimuth angle of the nanocomposite film for achieving the specific Bragg reflections in RSM measurements.

Table 1. Lattice parameters and angles of BaTiO₃ in bulk and thin films.

	Lattice parameter (Å, a)	Lattice parameter (Å, b)	Lattice parameter (Å, c)	Lattice angles (°)
BaTiO ₃ bulk ^[38]	3.9938	3.9938	4.0361	$\alpha, \beta, \gamma = 90$
Plain BaTiO ₃ 100 nm	3.995 ± 0.008	3.994 ± 0.006	4.065 ± 0.007	$\alpha, \beta, \gamma = 90$
BaTiO ₃ in 500 nm nanocomposite film	4.151 ± 0.005	4.135 ± 0.005	4.122 ± 0.007	$\alpha, \gamma = 90$ $\beta = 99.01$

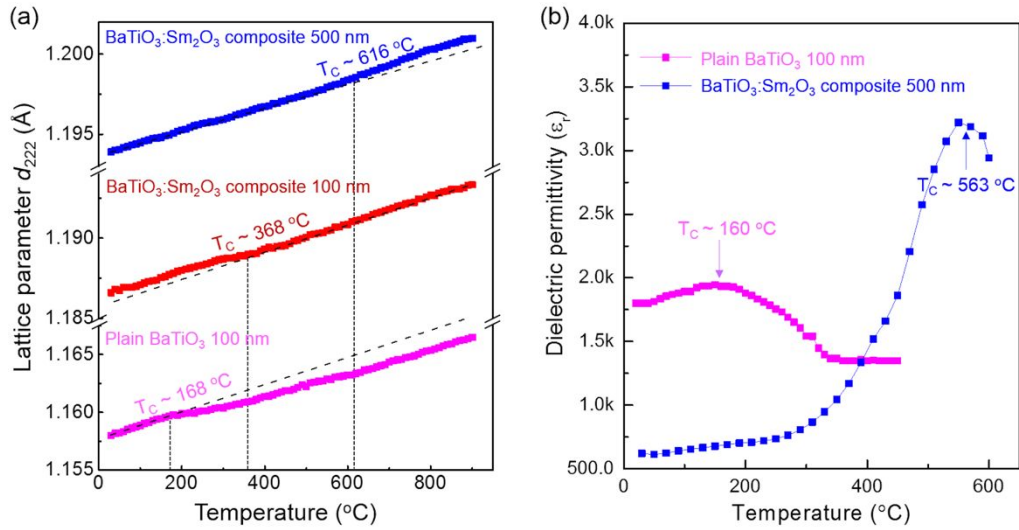


Figure 2. (a) Temperature dependent lattice parameter d_{222} of plain BaTiO₃ film and BaTiO₃:Sm₂O₃ nanocomposite films. Two distinct regimes separated by a kink in the lattice parameter are observed. (b) Dielectric permittivity of plain BaTiO₃ film and BaTiO₃:Sm₂O₃ nanocomposite film measured as a function of temperature at 50 kHz.

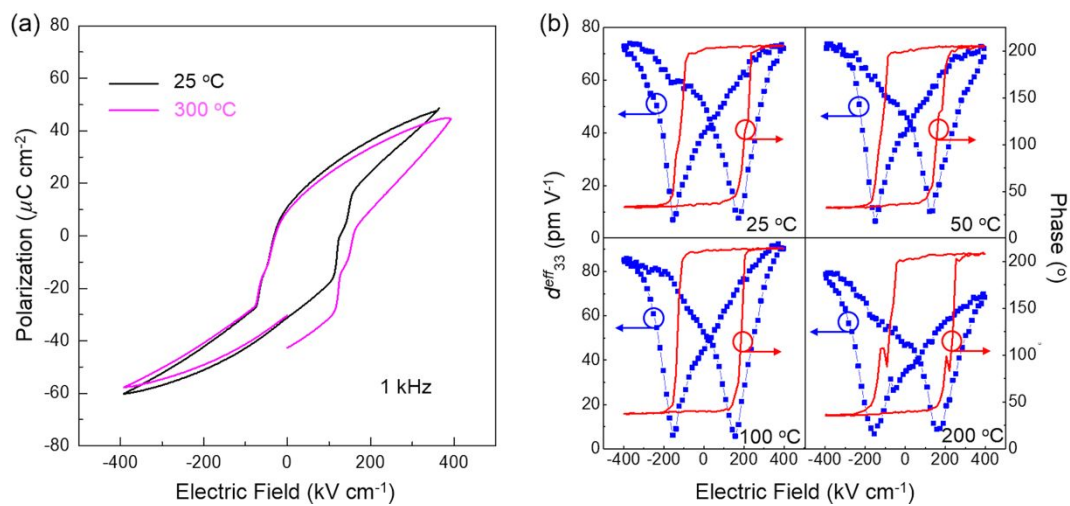


Figure 3. (a) Ferroelectric hysteresis loops of 500-nm-thick $\text{BaTiO}_3:\text{Sm}_2\text{O}_3$ nanocomposite film at 25 °C and 300 °C revealing the presence of strong and robust polarization even at 300 °C. (b) Effective piezoelectric coefficient d_{33}^{eff} and phase hysteresis loops of 500-nm-thick $\text{BaTiO}_3:\text{Sm}_2\text{O}_3$ nanocomposite film measured from 25 °C to 200 °C.

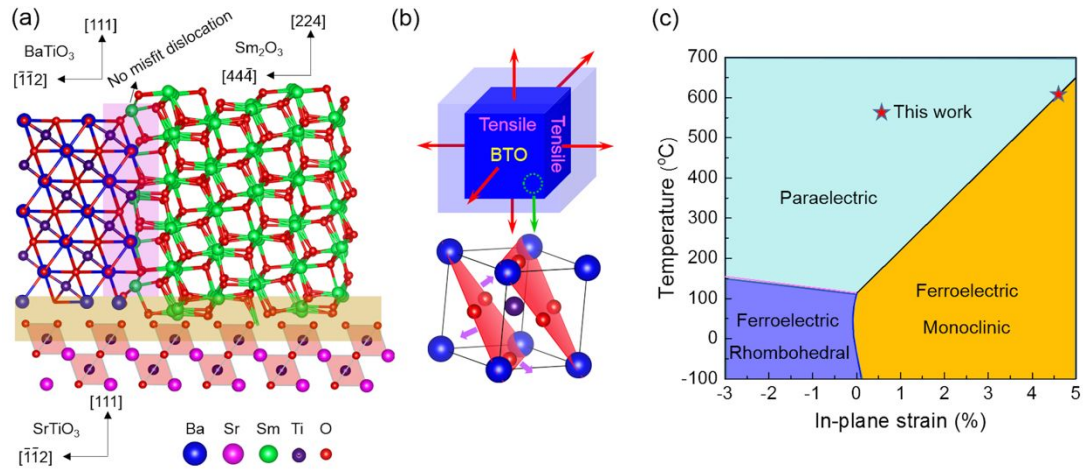


Figure 4. (a) Crystallographic model of a BaTiO₃:Sm₂O₃ nanocomposite film around vertical interface between BaTiO₃ and Sm₂O₃. (b) Schematic diagram of 3D tensile strain applied to BaTiO₃. The thin arrows in top panel represent the tensile strain applied along three mutually perpendicular directions. The thick arrows in bottom panel represent the three oxygen atoms around Ti atom move away from each other after applying 3D tensile strain. (c) Temperature-dependent in-plane strain phase diagram of (111)-oriented BaTiO₃ from theory calculation.²⁴ The star represents the ferroelectric Curie temperature of BaTiO₃ in 500-nm-thick nanocomposite film.

Negative pressure enhances the ferroelectric Curie temperature and piezoelectric coefficient in *lead-free* monoclinic BaTiO₃ films for high-temperature ferroelectric applications.

